

Three New Polyoxoniobates Functioning as Different Oxidation Catalysts

Ting-Ting Zhang, Guanghua Li, and Xiao-Bing Cui*



Cite This: <https://dx.doi.org/10.1021/acs.cgd.0c01193>



Read Online

ACCESS |



Metrics & More

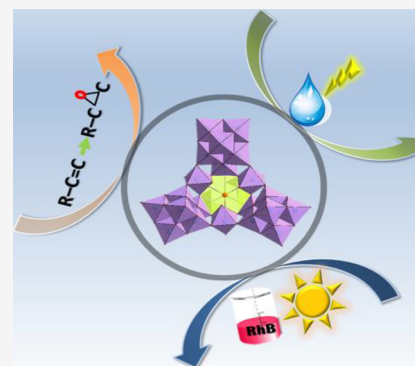


Article Recommendations



Supporting Information

ABSTRACT: Three new multifunctional isopolyoniobates based on $\{\text{Nb}_{24}\text{O}_{72}\}$, namely, $[\text{Cu}(\text{en})_2]_{9.75}[\text{Cu}(\text{en})_2(\text{H}_2\text{O})]_4[\text{KNb}_{24}\text{O}_{72}\text{H}_{9.25}]_2 \cdot 36.5\text{H}_2\text{O}$ (**1**), $[\text{Cu}(\text{en})_2][\text{Cu}(\text{en})_2(\text{H}_2\text{O})]_{12}[\text{Cu}(\text{en})_2(\text{H}_2\text{O})_2]_3[\text{KNb}_{24}\text{O}_{72}\text{H}_7(\text{H}_2\text{O})_2]_2 \cdot 99\text{H}_2\text{O}$ (**2**), and $[\text{K}(\text{H}_2\text{O})_4][\text{Cu}(\text{en})_2(\text{H}_2\text{O})_2]_5[\text{Cu}(\text{en})_2(\text{H}_2\text{O})]_{8.25}[\text{Cu}(\text{en})_2][\text{K}_{0.5}\text{Nb}_{24}\text{O}_{72}\text{H}_{7.75}]_2 \cdot 115.31\text{H}_2\text{O}$ (**3**) (en = ethylenediamine), were obtained and characterized by IR, powder X-ray diffraction, single-crystal diffraction analysis, etc. Single-crystal analyses of the three compounds shows that all their clusters exhibit the same bowl-shaped structure, while the different transition metal complexes (TMCs) make compounds **1–3** show three entirely different packing structures. The catalytic properties of the three compounds as catalysts for Rhodamine B (RhB) photocatalytic degradation, styrene oxidation, and oxygen evolution reaction (OER) have been assessed, and all the compounds have good catalytic effects on the three different catalytic processes.



INTRODUCTION

Polyoxometalates (POMs), as a series of unique inorganic compounds with diverse structures and fascinating applications, have been attracting more and more scientists' attention.^{1,2} Even though the chemistry of POMs has been known for more than two hundred years,¹ the evolution of the complex structures and multiple functions of POMs has been through a flourishing stage which is closely involved with many application fields such as catalysis, material science, biochemistry, analysis, and medicine.^{3–9} However, by now, POMs that were synthesized and studied have still been dominated by polyoxotungstates (POWs), polyoxomolybdates (POMos), and polyoxovanadates (POVs), no matter for isopolyoxometalates or heteropolyoxometalates. The main reason is that for POWs, POMos, or POVs, their cluster elements can aggregate readily in a wide pH range.^{10,11} In contrast, due to harsh synthesis conditions (the main precursor $\{\text{Nb}_6\text{O}_{19}\}$ is only stabilized in a highly alkaline solution), the study for polyoxoniobates (PONBs) is more slowly compared with other POMs.¹² However, in recent years, their unique structures and potential properties have made PONBs gradually become a hot topic in the inorganic chemistry field.¹³ Hence there are a growing number of scientists who devote to the study of PONBs, which can be applied especially in the fields of base catalysis,^{14,15} nuclear waste treatment,¹⁶ proton conduction,¹⁷ photolysis,¹⁸ magnetism,¹⁹ and anticancer.²⁰

Up to now, Keggin type PONBs are the most well-studied ones. One interesting feature on the reported Keggin type PONBs is that almost all of them have capped atoms, such as $\{[\text{Ti}_2\text{O}_2][\text{XNb}_{12}\text{O}_{40}]\}^{n-}$ (X = Si, Ge),^{12,21} $\{[\text{Nb}_2\text{O}_2]-$

$[\text{XNb}_{12}\text{O}_{40}]\}^{n-}$ (X = Si, Ge, V, P),^{12,21–24} $\{[\text{Sb}_2\text{O}_2]-[\text{XNb}_{12}\text{O}_{40}]\}^{n-}$ (X = Si, Ge, V, P, As),²⁵ $\{[\text{V}_2\text{O}_2]-[\text{XNb}_{12}\text{O}_{40}]\}^{n-}$ (X = Si, Ge, V, P),^{26–29} $\{[\text{V}_4\text{O}_4]-[\text{ASNb}_{12}\text{O}_{40}]\}^{7-}$,³⁰ $\{[\text{V}_6\text{O}_6][\text{PNb}_{12}\text{O}_{40}]\}^{3-}$,³¹ and $\{\text{Cu}(2,2'-\text{bipy})\}_6(\text{PNb}_{12}\text{O}_{40})\}^{3-}$.³² The differences between these Keggin clusters are the type and/or the number of the central and/or capped atoms. In addition, there also are a large number of studies focusing on the other types of PONBs, such as $\{[\text{Hg}(\text{cyclam})]_6\text{Nb}_6\text{O}_{19}\}(\text{NO}_3)_4 \cdot 14\text{H}_2\text{O}$,³³ $\{[\text{Cu}(\text{-phen})]_2[\text{Cu}(\text{phen})]_2\text{Nb}_6\text{O}_{19}\} \cdot 24\text{H}_2\text{O}$,³⁴ $\{\text{Nb}_6\text{O}_{19}[\text{Cu}(2,2'-\text{bipy})]_2[\text{Cu}(2,2'-\text{bipy})]_2\} \cdot 19\text{H}_2\text{O}$,³⁵ $\{[\text{Cu}(1,10\text{-phen})][\text{Cu}(1,10\text{-phen})(\text{H}_2\text{O})]\text{Nb}_6\text{O}_{19}\} \cdot 10.5\text{H}_2\text{O}$,³⁶ $\{[\text{Cu}(\text{cyclam})]_2[\text{HTiNb}_9\text{O}_{28}]\}^{2-}$,³⁷ $\text{K}_5[\text{Cu}(\text{H}_2\text{O})_2(\text{cyclam})]_{1.5}\{[\text{Cu}(\text{cyclam})][\text{Cu}(\text{H}_2\text{O})(\text{cyclam})]_2\text{HSiNb}_{18}\text{O}_{54}\}(\text{NO}_3)_3 \cdot 30\text{H}_2\text{O}$,³⁸ $\{[\text{Cu}(\text{cyclam})(\text{H}_2\text{O})]_2[\text{Cu}(\text{cyclam})][\text{Nb}_{10}\text{O}_{28}]\}_n \cdot n\text{H}_2\text{O}$,³⁸ $\{[\text{Ni}(\text{cyclam})]_4[\text{Ti}_2\text{Nb}_8\text{O}_{28}]\}_n \cdot \sim 28n\text{H}_2\text{O}$,³⁹ $\{[\text{Ni}(\text{cyclam})]_4[\text{Ti}_2\text{Nb}_8\text{O}_{28}]\}_n \cdot \sim 28n\text{H}_2\text{O}$,³⁹ $\text{K}[\text{Ni}(\text{cyclam})]_3[\text{TiNb}_9\text{O}_{28}] \cdot 14\text{H}_2\text{O}$,³⁹ $[\text{Nb}_{20}\text{O}_{54}]^{8-}$,⁴⁰ $[\text{Nb}_{10}\text{V}_4\text{O}_{40}(\text{OH})_2]^{12-}$,⁴¹ $[\text{Nb}_{24}\text{O}_{72}\text{H}_{21}]^{3-}$,⁴² $[\text{Nb}_{32}\text{O}_{96}\text{H}_{28}]^{4-}$,⁴² and $\text{K}_4@[\text{Cu}_{29}(\text{OH})_7(\text{H}_2\text{O})_2(\text{en})_8(\text{trz})_{21}][\text{H}_2\text{Nb}_{24}\text{O}_{69}(\text{H}_2\text{O})_3]_{30-43}$.

The first $\{\text{Nb}_{24}\}$ compound was reported in 2006. It was the first larger polyoxoniobate cluster with $[\text{Cu}(\text{en})_2]^{2+}$ as a

Received: August 30, 2020

Revised: April 1, 2021

Table 1. Crystal Data of Compounds 1–3

	compound 1	compound 2	compound 3
empirical formula	C ₅₅ H _{319.5} Cu _{13.75} K ₂ N ₅₅ Nb ₄₈ O _{184.5}	C ₆₄ H ₅₁₂ Cu ₁₆ K ₂ N ₆₄ Nb ₄₈ O ₂₆₅	C ₆₁ H _{534.62} Cu _{15.25} K ₂ N ₆₁ Nb ₄₈ O _{281.56}
formula weight	10116.69	11975.87	12137.94
crystal system	triclinic	triclinic	triclinic
space group	$P\bar{1}$	$P\bar{1}$	$P\bar{1}$
<i>a</i> /Å	18.0474(17)	19.760(3)	24.1930(14)
<i>b</i> /Å	20.4106(19)	21.980(3)	25.4019(15)
<i>c</i> /Å	20.454(2)	22.140(3)	33.981(2)
α /deg	93.669(3)	85.734(4)	109.940(2)
β /deg	102.211(3)	74.488(4)	95.720(2)
γ /deg	95.773(3)	81.434(4)	97.119(2)
<i>V</i> /Å ³	7298.4(12)	9156.3(19)	19253(2)
<i>Z</i>	1	1	2
<i>D_c</i> /mg m ⁻³	2.302	2.172	2.094
μ /mm ⁻¹	2.908	2.479	2.322
<i>F</i> (000)	4915.0	5934	12057
θ for data collection	2.33–25.16	2.426–25.198	2.299–25.027
no. of reflns collected	53 694	76 262	184 345
no. of unique reflns	24 717	32 206	67 737
<i>R</i> (int)	0.0400	0.0659	0.0459
completeness to θ	96.1	96.8	99.3
parameters	1904	2486	3922
GOF on <i>F</i> ²	1.095	1.023	1.026
<i>R</i> ^a [<i>I</i> > 2 σ (<i>I</i>)]	<i>R</i> ₁ = 0.0941	<i>R</i> ₁ = 0.0827	<i>R</i> ₁ = 0.0564
<i>R</i> ^b (all data)	<i>wR</i> ₂ = 0.2636	<i>wR</i> ₂ = 0.2465	<i>wR</i> ₂ = 0.1612

$$^a R_1 = \frac{\sum ||F_o| - |F_c||}{\sum |F_o|}, \quad ^b wR_2 = \left\{ \frac{\sum [w(F_o^2 - F_c^2)^2]}{\sum [w(F_o^2)^2]} \right\}^{1/2}.$$

transition metal complex (TMCs) to coordinate with the cluster at that time.⁴⁴ Niu's group then reported two {Nb₂₄} PONbs [Cu(en)₂]₃[Cu(en)₂(H₂O)]₉{[H₂Nb₆O₁₉]C-}[(K_{0.5}Nb₂₄O₇₂H_{10.25})]₂{Cu₃(en)₃(H₂O)₃}-[Na_{1.5}Cu_{1.5}(H₂O)₈]{Cu(en)₂}]₆·144H₂O and [Cu(en)₂]₃[Cu(en)₂(H₂O)]₁₅[K_{0.5}Nb₂₄O₇₂H_{14.5}]₂·25H₂O, of which the K atom is located at the center of the clusters.^{45,46}

In 2012, another two {Nb₂₄} compounds were reported by Wang's group, and they not only detailed the structures but also tested the photocatalytic H₂ evolution activities of their compounds.^{42,47} In 2019, Zheng et al. reported the first three representatives of a brand-new class of inorganic–organic hybrid PONbs: PONb–metal–complex cage materials, one of which is based on the {Nb₂₄} cluster.⁴³ All the PONbs mentioned above have the identical {Nb₂₄} cluster model. However, there is an exception: [H₂Te₂Nb₂₄O₇₂]¹⁴⁻ was reported by Niu's group in 2017, and its performance for decolorization of basic fuchsin has been studied.⁴⁸

In this work, we synthesized three new PONbs based on {Nb₂₄} clusters and [Cu(en)₂]²⁺ complexes: namely, [Cu(en)₂]_{9.75}[Cu(en)₂(H₂O)]₄[KNb₂₄O₇₂H_{9.25}]₂·36.5H₂O (**1**), [Cu(en)₂]₁₂[Cu(en)₂(H₂O)]₃·[KNb₂₄O₇₂H₇(H₂O)]₂·99H₂O (**2**), and [K(H₂O)]₄[Cu(en)₂(H₂O)]₅[Cu(en)₂(H₂O)]_{8.25}[Cu(en)₂][K_{0.5}Nb₂₄O₇₂H_{7.75}]₂·115.31H₂O (**3**). These compounds are not only characterized by FT-IR, PXRD, and single-crystal X-ray diffraction analysis but also studied as catalysts in three different catalytic systems. The results show that all three new compounds have remarkable performances for the different catalytic experiments.

EXPERIMENTAL SECTION

Materials and Methods. All the chemicals were of analytical reagent grade quality, purchased commercially, and used without further purification. K₇HfNb₆O₁₉·13H₂O was synthesized according to the literature⁴⁹ and characterized by an IR spectrum. Fourier transform infrared spectra were recorded using a PerkinElmer Spectrum One FT-IR spectrophotometer and the samples were prepared as KBr pellets. UV–vis spectra were obtained using a Shimadzu UV-3100 spectrophotometer. X-ray diffraction (XRD) measurements were performed by using a Cu K α source on a powder diffractometer (Scintag X1). Elemental analyses for C, H, and N were performed on a PerkinElmer 2400 CHN elemental analyzer. The chemical compositions of the samples were determined by inductively coupled plasma–optical emission spectroscopy (PerkinElmer Optima 3300DV). The electrochemical measurements were conducted on a CHI 760e electrochemical workstation.

Synthetic Procedures. [Cu(en)₂]_{9.75}[Cu(en)₂(H₂O)]₄·[KNb₂₄O₇₂H_{9.25}]₂·36.5H₂O (**1**). Compound **1** was synthesized by the evaporation method. The mixture of 8 mL of Na₂CO₃/NaHCO₃ (0.5M, pH = 10) buffer solution, K₇HfNb₆O₁₉·13H₂O (0.35g, 0.26 mmol), CuCl₂·2H₂O (0.20g, 0.12 mmol), Na₂SiO₃·9H₂O (0.02g, 0.06 mmol), Sb₂O₃ (0.03g, 0.10 mmol), and en (0.15 mL) was stirred for 3 h. Then the resulting solution was filtered, and the filtrate was slowly evaporated at room temperature. Deep purple single crystals were obtained after 7 days. Yield: 42% based on Nb. Anal. Calcd for C₅₅H_{319.5}Cu_{13.75}K₂N₅₅Nb₄₈O_{184.5}: Nb, 44.08; Cu, 8.64; K, 0.77; C, 6.53; N, 7.62; H, 3.18. Found: Nb, 44.02; Cu, 8.53; K, 0.81; C, 6.46; N, 7.69; H, 3.02.

[Cu(en)₂]₁₂[Cu(en)₂(H₂O)]₃[KNb₂₄O₇₂H₇(H₂O)]₂·99H₂O (**2**). Compound **2** was synthesized using the procedure very similar to that of compound **1**, except that the amount of K₇HfNb₆O₁₉·13H₂O was changed to (0.25 g, 0.18 mmol). Deep purple single crystals were obtained after 10 days. Yield: 31% based on Nb. Anal. Calcd for C₆₄H₅₁₂Cu₁₆K₂N₆₄Nb₄₈O₂₆₅: Nb, 37.24; Cu, 8.49; K, 0.65; C, 6.42; N, 7.49; H, 4.31. Found: Nb, 37.11; Cu, 8.40; K, 0.53; C, 6.45; N, 7.50; H, 4.41.

[K(H₂O)]₄[Cu(en)₂(H₂O)]₅[Cu(en)₂(H₂O)]_{8.25}[Cu(en)₂][K_{0.5}Nb₂₄O₇₂H_{7.75}]₂·115.31H₂O (**3**). Compound **3** was synthesized with a combined hydrothermal and evaporation method. The mixture of 8

mL of $\text{Na}_2\text{CO}_3/\text{NaHCO}_3$ (0. , pH = 10) buffer solution, $\text{K}_7\text{HfNb}_6\text{O}_{19} \cdot 13\text{H}_2\text{O}$ (0.25 g, 0.18 mmol), $\text{Cu}(\text{AC})_2 \cdot \text{H}_2\text{O}$ (0.13 g, 0.65 mmol), $\text{Na}_3\text{AsO}_4 \cdot 12\text{H}_2\text{O}$ (0.013 g, 0.06 mmol), Sb_2O_3 (0.01 g, 0.03 mmol), en (0.25 mL), and KCl (0.05 g, 0.67 mmol) was stirred for 3 h, and the pH of the mixture was necessarily adjusted to 12.5 with KOH (2 M) solution. The mixture was transferred into an 18 mL Teflon-lined autoclave and heated under autogenous pressure at 140 °C for 5 days and then left to cool to room temperature. After that, the resulting solution was filtered and the filtrate was slowly evaporated at room temperature. Deep purple single crystals were obtained after 10 days. Yield: 55% based on Nb. Anal. Calcd for $\text{C}_{61}\text{H}_{534.6}\text{Cu}_{15.25}\text{K}_2\text{N}_{61} \cdot \text{Nb}_{48}\text{O}_{281.6}$: Nb, 36.74; Cu, 7.98; K, 0.64; C, 6.04; N, 7.04; H, 4.41. Found: Nb, 36.58; Cu, 7.95; K, 0.56; C, 6.06; N, 7.00; H, 4.20.

X-ray Crystallography. The single-crystal diffraction data of compounds 1–3 were obtained on a Bruker Smart-CCD diffractometer with a Mo $K\alpha$ radiation ($\lambda = 0.71073 \text{ \AA}$). The data collected temperatures are 300(2), 211(2), and 200(2) K for compounds 1–3, respectively. In no data collection was evidence for crystal decay encountered. The three structures were solved by direct methods and refined using full-matrix least-squares method on F^2 using the SHELXTL-2014/7 program^{50,51} incorporated into the program package Olex2.⁵² In final refinements, all non-hydrogen atoms were refined with anisotropic displacement parameters except about 70 water molecules in compound 3, for there are too many atoms to be refined anisotropically even using the XH software. The hydrogen atoms of en ligands were placed in idealized positions and refined as rigid atoms with the relative isotropic displacement parameters, while hydrogen atoms of water molecules were not found from a difference Fourier map and not included in the calculation. In addition, there are also some hydrogens attached on cluster shells of the three compounds for balancing the charge of the compounds. Unfortunately, these plausible hydrogens cannot be located in the difference Fourier maps. We also conduct the BVS calculations for attempting to locate the exact positions of these hydrogens but not successfully. We think these hydrogens attached on the cluster shells should be distributed disorderedly. Therefore, the numbers of the proposed H atoms of the chemical formula of the three compounds are determined on the basis of the chemical analyses and the charge balancing requirements of the formula. Some undissolved A- and/or B-Alerts have been explained as validation reply forms in the CIF files. One copper complex in compound 1 is severely disordered, and the disordered model is depicted in Figure s1. Crystal data are listed in Table 1. CCDC numbers: 2021807 for compound 1, 2021808 for compound 2, and 2021809 for compound 3.

RESULTS AND DISCUSSION

Crystal Structure of Compound 1. Since the three compounds include almost the same cluster anions, here the anion of compound 1 is described in detail as an example (Figure 1). The shape of the cluster is like a “bowl”; it consists of three $\{\text{Nb}_6\text{O}_{19}\}$ clusters that serve as the top “bowl” edges and a cyclic $\{\text{Nb}_6\text{O}_{30}\}$ fragment serving as the bottom of the “bowl”. In addition to that, there is a K^+ located at the center of the $\{\text{Nb}_6\text{O}_{30}\}$ fragment (Figure 1). The “bowl” anion has 24 Nb atoms and interesting coordination patterns. There are three types of oxygens in the $\{\text{Nb}_6\text{O}_{19}\}$: terminal oxygens with Nb– O_t distances of 1.76(1)–1.86(1) Å, central oxygens with Nb– O_c distances of 2.25(1)–2.47(1) Å, and bridging oxygens with Nb– O_b distances of 1.87(1)–2.13(1) Å. It is worth mentioning that due to the participation of the $\{\text{Nb}_6\text{O}_{30}\}$, the distances of Nb– O_t and Nb– O_b involved in the connections have been lengthened to a certain extent.

As for the cyclic $\{\text{Nb}_6\text{O}_{30}\}$ fragment, its six $\{\text{NbO}_6\}$ octahedra can be divided into two three-member groups: A-group and B-group (Figure s2). As we can see, each Nb from the A- and B-groups are connected alternately by sharing two oxygens. Each Nb of the A-group coordinates with three

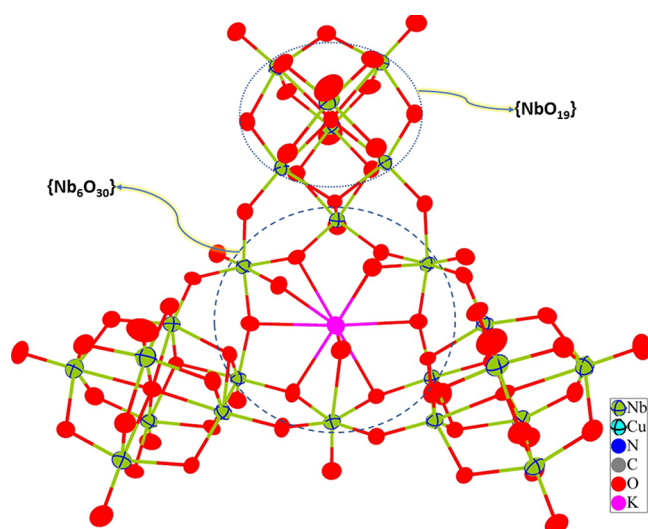


Figure 1. Ellipsoid representation of the bowl-shaped $[\text{KNb}_{24}\text{O}_{72}\text{H}_{9.25}]^{13.75-}$ anion in compound 1.

bridging O_b atoms from its corresponding $\{\text{Nb}_6\text{O}_{19}\}$ cluster, two bridging O_b atoms shared by two $\{\text{NbO}_6\}$ octahedra of the B-group, and a terminal O_t atom, while each Nb of the B-group is connected to two O_b atoms shared by two adjacent $\{\text{Nb}_6\text{O}_{19}\}$ clusters, two O_b atoms shared by two $\{\text{NbO}_6\}$ octahedra of the A-group and two terminal oxygens. There are only two kinds of oxygens in the $\{\text{Nb}_6\text{O}_{30}\}$, which are terminal oxygens with Nb– O_t distances of 1.72(1)–2.52(1) Å and bridging oxygens with Nb– O_b distances of 1.93(1)–2.29(1) Å. Due to the longer distance of the K–O, the K^+ is nine-coordinated with six bridging oxygen atoms and three terminal oxygen atoms with K–O distances of 2.74(1)–3.14(1) Å.

Single-crystal analysis suggests that compound 1 crystallizes in the $P\bar{1}$ space group. The asymmetric unit is composed of a $[\text{KNb}_{24}\text{O}_{72}\text{H}_{9.25}]^{13.75-}$, 4.875 $[\text{Cu}(\text{en})_2]^{2+}$, 2 $[\text{Cu}(\text{en})_2(\text{H}_2\text{O})]^{2+}$, and 18.25 lattice water molecules. The crystallographically independent copper atoms form two different types of complexes: $[\text{Cu}(\text{en})_2(\text{H}_2\text{O})]^{2+}$ and $[\text{Cu}(\text{en})_2]^{2+}$. The copper center of the former exhibits a distorted square-pyramidal geometry with four nitrogens coming from two en and one oxygen coming from a water molecule with Cu–N distances of 1.92(2)–2.14(4) Å and Cu–O distances of 2.17(3)–2.7872(2) Å. As for $[\text{Cu}(\text{en})_2]^{2+}$, the copper showing a square-planar geometry is only bonded to four nitrogens coming from two en ligands with comparable Cu–N distances. The $[\text{Cu}(\text{en})_2]^{2+}$ can be further classified into three subgroups based on contacts of the copper centers and oxygens from $[\text{KNb}_{24}\text{O}_{72}\text{H}_{9.25}]^{13.75-}$. The Cu(3), Cu(4), Cu(5), and Cu(8) coppers belong to the first subgroup, each copper of them not only shows interactions with four nitrogens originating from two en ligands but also has strong contacts with oxygens from $[\text{K}_{0.5}\text{Nb}_{24}\text{O}_{72}\text{H}_{7.75}]^{13.75-}$, presenting also a distorted square-pyramidal geometry. The Cu(6) copper form the second subgroup, interacting with two oxygens originating from two neighboring $[\text{K}_{0.5}\text{Nb}_{24}\text{O}_{72}\text{H}_{7.75}]^{13.75-}$ as well as four nitrogens coming from two en ligands. Therefore, Cu(6) serve as an inorganic bridge joining two $[\text{K}_{0.5}\text{Nb}_{24}\text{O}_{72}\text{H}_{7.75}]^{13.75-}$ to form a dimer, while Cu(3), Cu(4), Cu(5), and Cu(8) complexes are only supported by $[\text{K}_{0.5}\text{Nb}_{24}\text{O}_{72}\text{H}_{7.75}]^{13.75-}$ to form the POM-supported complex (Figure 2). The two remaining Cu(9) and Cu(10) (Cu(11)) complexes belong to

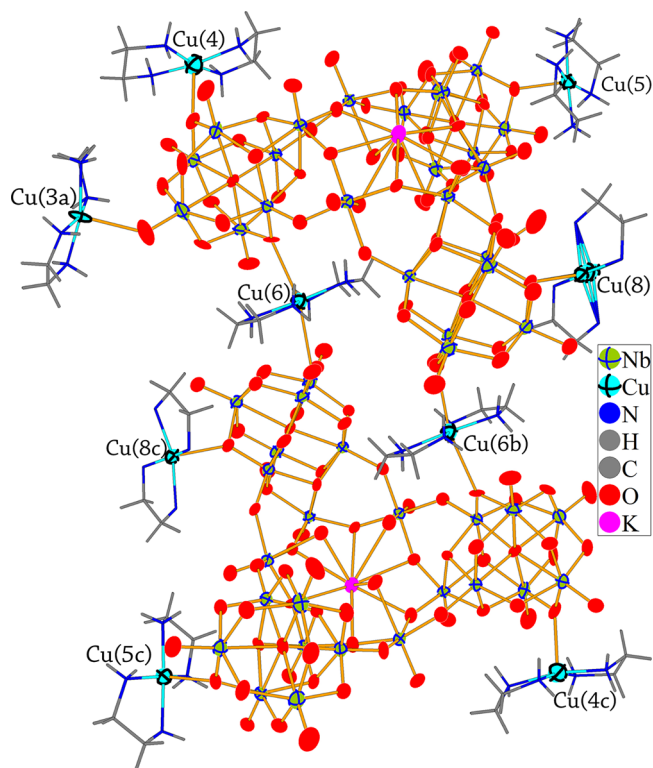


Figure 2. Ellipsoid representation of the dimer of the $[\text{KNb}_{24}\text{O}_{72}\text{H}_{9.25}]^{13.75-}$ cluster and its supported complexes in compound 1. $a(-x, -1 - y, -z)$; $b(-1 + x, -1 + y, -1 + z)$; $c(-x, -2 - y, -1 - z)$.

the third group, which has no contacts with any clusters. The Cu–O and Cu–N distances involving $[\text{Cu}(\text{en})_2]^{2+}$ complexes are all comparable to those of $[\text{Cu}(\text{en})_2(\text{H}_2\text{O})]^{2+}$ complexes.

Crystal Structure of Compound 2. The cluster structure of compound 2 is almost coincident with that of compound 1 except for the coordination environment of the K^+ . Here, the central K^+ is ten-coordinated by six bridging oxygen atoms, two terminal oxygen atoms from the cyclic $\{\text{Nb}_6\text{O}_{30}\}$ fragment, and two water molecules with K–O distances of 2.76(2)–3.315(8) Å.

As for the transition metal complexes in the asymmetric unit, there are three different kinds of Cu–en complexes: $[\text{Cu}(\text{en})_2]^{2+}$, $[\text{Cu}(\text{en})_2(\text{H}_2\text{O})]^{2+}$, and $[\text{Cu}(\text{en})_2(\text{H}_2\text{O})_2]^{2+}$. The third kind of complex, $[\text{Cu}(\text{en})_2(\text{H}_2\text{O})_2]^{2+}$, did not emerge in compound 1. Cu(4) and Cu(6) of the third kind of complex, $[\text{Cu}(\text{en})_2(\text{H}_2\text{O})_2]^{2+}$, display the octahedral environment formed by four nitrogens originating from two en ligands and two oxygens coming from two water molecules. The second kind of complex includes the majority of the copper ones, which are Cu(1), Cu(1b), Cu(3), Cu(5), Cu(7), Cu(8), Cu(9), Cu(10), and Cu(11) complexes in compound 2, each adopting a square-pyramidal geometry formed by four nitrogens originating from two en and an oxygen coming from a water molecule. It is worth noting that Cu(7) and Cu(10) of the second kind each coordinate with a terminal oxygen from $[\text{KNb}_{24}\text{O}_{72}\text{H}_7(\text{H}_2\text{O})_2]^{16-}$, as well as four nitrogens of two en and an oxygen of a water molecule, indicating that Cu(7) and Cu(10) complexes were supported by $[\text{KNb}_{24}\text{O}_{72}\text{H}_7(\text{H}_2\text{O})_2]^{16-}$ (Figure 3). There is one copper Cu(2) belonging to the first kind of complex, $[\text{Cu}(\text{en})_2]^{2+}$. All the Cu–N and Cu–O distances involving Cu–en complexes

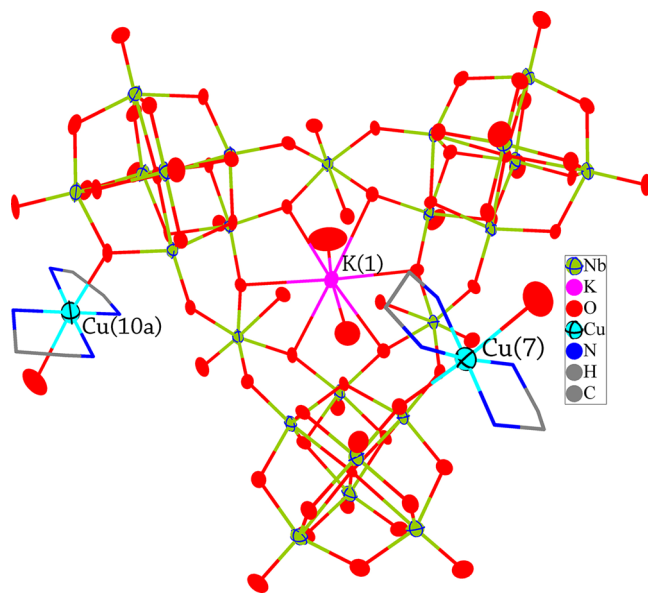


Figure 3. Ellipsoid representation of the $[\text{KNb}_{24}\text{O}_{72}\text{H}_7(\text{H}_2\text{O})_2]^{16-}$ cluster and its supported complexes in compound 2. $a(2 - x, 2 - y, 1 - z)$.

in compound 2 are comparable to those in compound 1. In addition to this, there are 49.5 lattice water molecules filling the space of the asymmetric unit of compound 2.

Crystal Structure of Compound 3. The cluster structure of compound 3 is almost identical to that of compound 1 with only a slight differences in bond lengths and angles. In the asymmetric unit of compound 3, there are two crystallographically different $[\text{K}_{0.5}\text{Nb}_{24}\text{O}_{72}\text{H}_{7.75}]^{15.75-}$ clusters. Also, the transition metal complexes of compound 3 can be classified into three groups: $[\text{Cu}(\text{en})_2]^{2+}$, $[\text{Cu}(\text{en})_2(\text{H}_2\text{O})]^{2+}$, and $[\text{Cu}(\text{en})_2(\text{H}_2\text{O})_2]^{2+}$. As in compounds 1 and 2, the group $[\text{Cu}(\text{en})_2(\text{H}_2\text{O})_2]^{2+}$ also occupies the majority of the transition metal complexes in compound 3, including Cu(0a), Cu(3), Cu(6), Cu(7), Cu(8), Cu(12), Cu(13), Cu(14), and Cu(16) ones, each copper of which has a square-pyramidal environment formed by four nitrogens coming from two en and an oxygen coming from a water molecule. In contrast to compounds 1 and 2, the number of $[\text{Cu}(\text{en})_2(\text{H}_2\text{O})_2]^{2+}$ groups is much larger than those in compound 2. There are five such crystallographically different copper complexes in the asymmetric unit of compound 3. They are Cu(4), Cu(5), Cu(9), Cu(11), and Cu(15) complexes, each copper of which is bonded to four nitrogen atoms coming from two en ligands and two oxygens originating from two water molecules. The $[\text{Cu}(\text{en})_2]^{2+}$ group includes only Cu(2), Cu(10), and Cu(17), each copper of which is chelated by two en ligands. Cu(10) is somewhat different among the members of the $[\text{Cu}(\text{en})_2]^{2+}$ group, coordinating with two oxygens from two neighboring $[\text{K}_{0.5}\text{Nb}_{24}\text{O}_{72}\text{H}_{7.75}]^{15.75-}$ besides the four nitrogens from two en ligands. Therefore, Cu(10) serves as an inorganic bridge connecting two clusters to form a dimer. In addition, Cu(13) and Cu(16) of the $[\text{Cu}(\text{en})_2(\text{H}_2\text{O})_2]^{2+}$ group are also somewhat different in comparison with the other members of this group; each of the two is supported by $[\text{K}_{0.5}\text{Nb}_{24}\text{O}_{72}\text{H}_{7.75}]^{15.75-}$ to form a POM-supported complex (Figure 4). All the Cu–N and Cu–O distances in compound 3 are very similar to those in compounds 1 and 2.

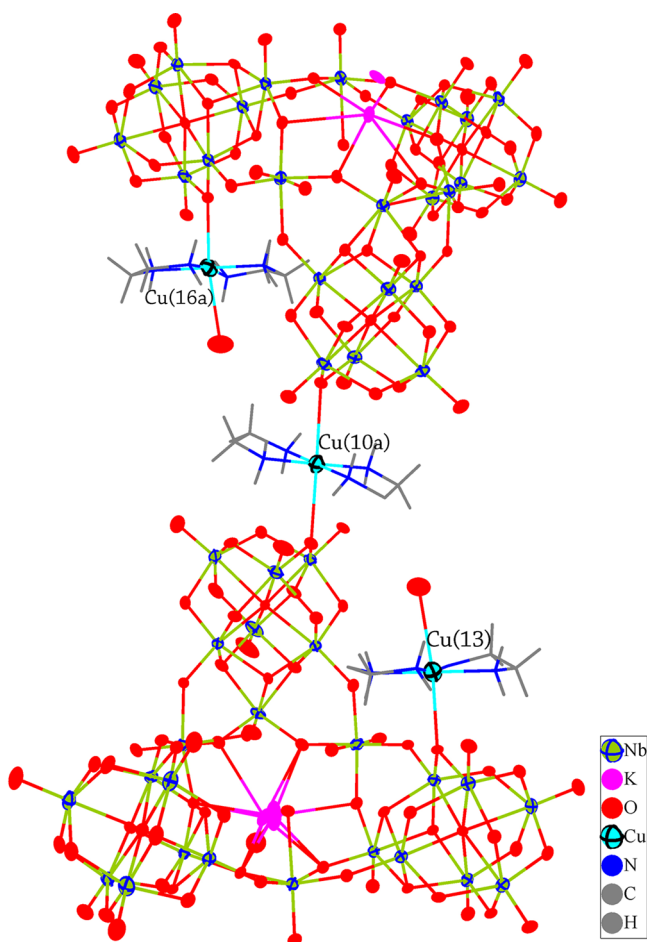


Figure 4. Ellipsoid representation of the dimer of $[\text{K}_{0.5}\text{Nb}_{24}\text{O}_{72}\text{H}_{7.75}]^{15.75-}$ cluster and its supported complexes in compound 3. $a(-1+x, y, z)$.

It is noteworthy that there has been a reported PONb compound with cell parameters very similar to those of compound 3.⁴⁷ However, the formula of the reported compound is $[\text{Cu}(\text{en})_2]_{11}\text{K}_4\text{Na}_2[\text{KNb}_{24}\text{O}_{72}\text{H}_9]_2 \cdot 120\text{H}_2\text{O}$, which is thoroughly different from that of compound 3: $([\text{K}(\text{H}_2\text{O})_4]_4[\text{Cu}(\text{en})_2(\text{H}_2\text{O})_2]_5[\text{Cu}(\text{en})_2(\text{H}_2\text{O})]_{8.25}[\text{Cu}(\text{en})_2]_2[\text{K}_{0.5}\text{Nb}_{24}\text{O}_{72}\text{H}_{7.75}]_2 \cdot 115.31\text{H}_2\text{O}$ (3) can be rewritten as $[\text{Cu}(\text{en})_2]_{15.25}\text{K}[\text{K}_{0.5}\text{Nb}_{24}\text{O}_{72}\text{H}_{7.75}]_2 \cdot 137.56\text{H}_2\text{O}$ (3) according to the formula fashion reported previously as mentioned above. Obviously, compound 3 and the reported one fell into two distinct compounds.

Syntheses and Discussion. Compounds 1 and 2 were synthesized with the evaporation method. Compared with the hydrothermal method, the lower temperature of the evaporation method leads to a slower nucleation speed so that evaporation synthesis is easy to generate some high-nuclear compounds.⁵³ In contrast, compound 3 was synthesized with the combination of the hydrothermal and the evaporation methods, and the combination could better integrate the advantages of the two methods, thereby synthesizing more crystals with diversified structures and functions. In the synthesis of compounds 1–3, $\text{Na}_2\text{SiO}_3 \cdot 9\text{H}_2\text{O}$, Sb_2O_3 , and $\text{Na}_3\text{AsO}_4 \cdot 12\text{H}_2\text{O}$ were used as starting materials; unfortunately, all of them are not incorporated into the final compounds. Even so, they are still necessary for the formation of our compounds. One or more starting materials that were

not incorporated into the final products were often observed in the inorganic synthesis process.⁵⁴

Characterization. The cluster structures of compounds 1–3 are almost identical, and all of them have $[\text{Cu}(\text{en})_n(\text{H}_2\text{O})_m]^{2+}$ ($n = 1$ or 2 , $m = 0, 1$, or 2) as metal complexes. Therefore, their FT-IR signatures are very similar to each other. The FT-IR spectroscopic characteristics of compound 1 as an example are described in detail. The IR spectrum of compound 1 is depicted in Figure s3. The medium strong peak at the band of 3138 cm^{-1} is ascribed to the $\nu(\text{H}-\text{O})$ frequency, the characteristic medium strong band at 898 cm^{-1} is attributed to the $\nu(\text{Nb}-\text{O}_t)$ frequency, and the strong band at 785 cm^{-1} and medium strong bands at 655 and 527 cm^{-1} are due to $\nu(\text{Nb}-\text{O}_b-\text{Nb})$ frequencies. The bands at 1588 – 1045 cm^{-1} correspond to vibration frequencies of en ligands in compound 1 ($1588(\text{m})$ and $1045(\text{m})$ for $\nu(\text{C}-\text{N})$, $1428(\text{m})$ for $\nu(\text{C}-\text{C})$). Both the FT-IR spectra of compounds 2 and 3 are somewhat similar to that of compound 1, having frequencies at $876(\text{m})$, $779(\text{m})$, $648(\text{w})$, and $537(\text{w})\text{ cm}^{-1}$ for 2 and $871(\text{m})$, $746(\text{s})$, $654(\text{m})$, and $522(\text{m})\text{ cm}^{-1}$ for 3 ascribed to $\nu(\text{Nb}-\text{O}_t)$ and $\nu(\text{Nb}-\text{O}_b-\text{Nb})$, respectively.

The X-ray powder diffraction patterns of compounds 1–3 are all consistent with the simulated XRD patterns, confirming the phase purity of all three compounds (Figure s4). The differences in reflection intensities are probably due to the preferential orientations in the powder samples of compounds 1–3.

As a classical organic pollutant, RhB (Rhodamine B) degradation^{55,56} under simulated solar light irradiation is used to assess the photocatalytic properties of materials. For a long time, many scientists have committed themselves to the purification of wastewater with POMs.^{57–59} However, the photocatalytic performance toward RhB degradation with $[\text{Cu}(\text{en})_2]^{2+}$ –PONbs as catalysts is seldom explored, although the copper(II)–ethylenediamine complex presents a strong adsorption ability in the visible light region.⁴⁴ Here, we take RhB as the organic pollutant of wastewater to investigate the photocatalytic activities of compounds 1–3 under simulated solar light irradiations. The photocatalytic performances of compounds 1–3 have been tested in a typical process; the ground catalyst powder (5 mg) was equally dispersed in the solution of RhB (100 mL, $1.0 \times 10^{-5}\text{ M}$). In the dark after being stirred magnetically for 30 min, the suspension was finally exposed to irradiation from a 400 W Xe lamp at the distance of about 4–5 cm between the liquid surface and the lamp. And the suspension was stirred at a stirring rate of 790–800 rpm with the irradiation. At 30 min intervals, 4 mL of the sample was taken out using a syringe, then centrifuged at 10 000 rpm for 5 min, and finally analyzed by using UV–vis spectroscopy (Figure s5). The blank experiment (without catalyst) shows that only 8.17% of RhB was photodegraded after 360 min. The plots of C_t/C_0 versus time for RhB solutions are shown in Figure s5. From the results, we can see that all three compounds possess photocatalytic properties to degrade RhB compared with the blank experiment. For compounds 1–3, compound 1 has the best activity with the degradation of RhB of 40.28%, while the degradations of RhB over compounds 2 and 3 are 25.22% and 25.45%, respectively, under simulated solar light irradiations.

The POM as a powerful catalyst has an excellent performance for the selective oxidation in organic reactions.^{60–63} With the deepening of the PONb research, scientists have reported some PONbs as organic reaction

Table 2. Selectivities and Conversions of Compounds 1–3 at 80 °C^a

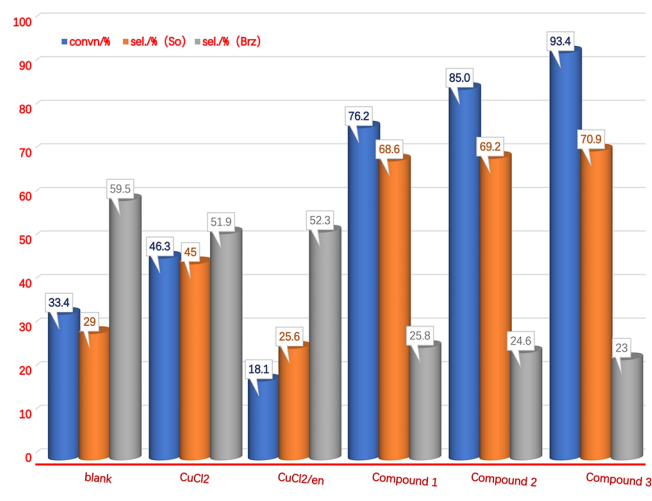
	catalyst	convn/%	sel/(% (So))	sel/(% (Brz))	sel/(% (others))	TOF
1	blank	33.4	29.0	59.5	11.5	
2	CuCl ₂	46.3	45.0	51.9	3.1	
3	CuCl ₂ /en	18.1	25.6	52.3	22.1	
4	compound 1	76.2	68.6	25.8	5.6	480.8
5	compound 2	85.0	69.2	24.6	6.2	636.2
6	compound 3	93.4	70.9	22.9	6.2	707.8

^aSo: styrene oxide. Bza: benzaldehyde. Others: including benzoic acid and phenylacetaldehyde.

catalysts.^{64,65} Compared with other POMs, there is still a large space for the catalysis study of PONbs. For a long time, the oxidation of olefins has been an important process due to the demand of the epoxides in the chemical industry.^{66–68} Here, we take compounds 1–3 as the catalysts to test their catalytic ability for the oxidation of styrene. The experimental epoxidations of styrene to styrene oxide were conducted in a batch reactor using aqueous *tert*-butyl hydroperoxide (TBHP) as the oxidant and compounds 1–3 as the catalysts. In a typical run, the catalyst (compound 1 (2 mg, 0.20 μmol), compound 2 (2 mg, 0.17 μmol), and compound 3 (2 mg, 0.16 μmol)), 0.114 mL (1 mmol) of styrene as the substrate, and 2 mL of CH₃CN were transferred into a two-neck round-bottom flask (5 mL) equipped with a magnetic stirrer and a reflux condenser. The mixture was heated to 60 or 80 °C, and then 1 mmol of TBHP as the oxidant was added. The addition of the TBHP was taken as the start of the catalytic reaction. The evolutions of the catalytic reactions were monitored using a gas chromatograph (Shimadzu, GC-8A) equipped with a FID detector and an HP-5 capillary column. Reaction products were identified by GC–MS (Shimadzu GCMS-QP 2010 Plus). The activity of the reaction system without the catalysts was determined.

Table 2 and Scheme 1 show the catalytic activities for styrene epoxidations over different catalysts at 80 °C. As

Scheme 1. Catalytic Activities and Product Distributions



expected, the three catalysts are all active for the styrene epoxidations using TBHP. Compound 1 shows the catalytic performance with 76.2% conversion and the styrene oxide selectivity of 68.6% after 8 h (Table 2, entry 4). Compound 2 shows the catalytic activity with 85.0% conversion and the styrene oxide selectivity of 69.2% (Table 2, entry 5). The styrene conversion and the styrene oxide selectivity of

compound 3 are 93.4% and 70.9% (Table 2, entry 6). From these data, we can see that for this PONb catalytic system, compound 3 as the catalyst has the best catalytic performance no matter the conversion or selectivity. By contrast, compound 1 has the lowest activity compared with the other two. From the catalytic performances and the molecular formula of compounds 1–3, we speculate that maybe the number of the copper complexes [Cu(en)_n(H₂O)_m]²⁺ (*n* = 1 or 2, *m* = 0, 1, or 2) plays a key role for the catalytic properties of the three. Compounds 2 and 3 include more copper complexes per formula, and the two exhibit superior performances than compound 1. However, whether using the CuCl₂ or CuCl₂/en as catalyst (Table 2, entries 2 and 3), we do not have good catalytic activity, and the conversion even becomes lower than the blank when we use CuCl₂/en as the catalyst (Table 2, entry 3). The higher selectivity to the others than to the styrene oxide and benzaldehyde may indicate that the en ligand may trigger another reaction; thus the aim reaction has been restrained (Table 2, entry 3).

To further understand the catalytic properties of these compounds, compound 1, which is easier to resynthesize, as an example, has been tested in the same catalytic system but at different temperatures and using different catalyst dosages, and the result is shown in Table 3. It can be observed that the reaction temperature is an important factor affecting this catalytic system, the conversion is much higher at 80 °C than at 60 °C. The interesting thing is that the different temperature makes a different selectivity (Table 3, entries 3 and 5), the higher temperature improves the production of the styrene oxide in this catalytic system. While at the lower temperature, the main product is benzaldehyde. Otherwise, the selectivity to others except the styrene oxide and the benzaldehyde is reduced at the lower temperature. As for the influence of the catalyst dosage, we can see that from 2 to 5 mg the conversion increased from 51.4% to 66.1% at 60 °C (Table 3, entries 3 and 4). But the results using 2 mg and 10 mg at 80 °C are quite different; the conversion did not become higher with the increase of the catalyst dosage but decreased from 76.2% to 60.4% (Table 3, entries 5 and 6). The consequence shows that increasing a suitable catalyst dosage may improve the conversion but too much catalyst will have the opposite effect. The reason may be that the catalyst may react with the oxidant and thus consume some of the oxidants.^{69,70}

The heterogeneity or homogeneity of the catalyst of compound 1 was tested by a hot filtration experiment (Figure S5). Four hours later, the solution was filtered three times through the filtering membrane. The data showed that the reaction did not stop even without the catalyst in the catalytic system, meaning that although compound 1 is not completely dissolved in the solution, some of it still dissolved and can continue the catalytic process. The catalytic reaction is considered to be homogeneous in nature when ΔFilt/Δcat

Table 3. Selectivity and Conversion of Compounds 1 with Different Temperatures and Dosages^a

	dosage/mg	T/°C	convn/%	sel/(So)	sel/(Brz)	sel/(others)	TOF
1	blank-1	80	33.4	29.0	59.5	11.5	
2	blank-2	60	1.4	30.9	69.1	0.0	
3	2	60	51.4	14.5	83.0	2.5	324.5
4	5	60	66.1	18.8	79.2	2.1	167.2
5	2	80	76.2	68.6	25.8	5.6	480.8
6	10	80	60.4	60.6	31.5	8.0	76.4

^aSo: styrene oxide. Bza: benzaldehydel. Others: including benzoic acid and phenylacetaldehyde.

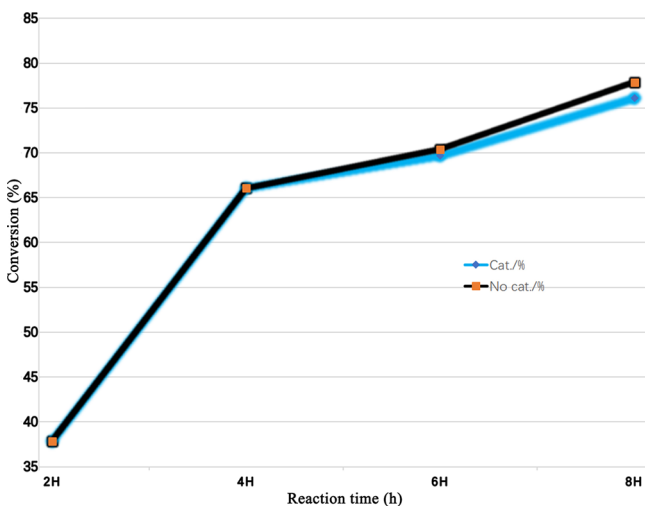
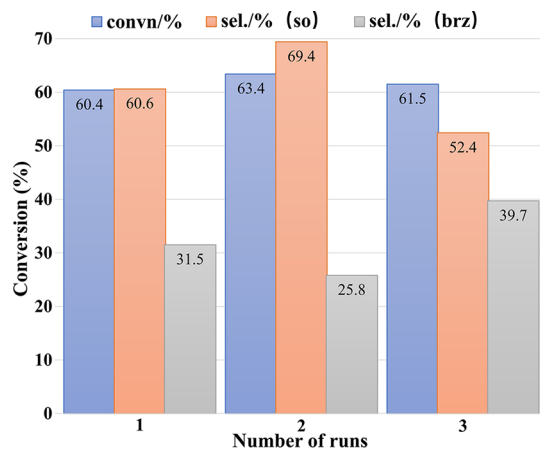


Figure 5. Result of the hot filtration test of compound 1.

$\cong 1$, where ΔFilt is the increment in olefin conversion in the time interval 4–8 h for the reaction carried out using the filtered solution and Δcat is the increment in olefin conversion during the same time interval for the reaction carried out in the presence of compound 1.⁷¹ Here, our $\Delta\text{Filt}/\Delta\text{cat}$ equals about 0.84; such a result suggests that compound 1 is a homogeneous catalyst for the epoxidation of styrene with TBHP.^{71–75} The catalyst is not completely dissolved in the catalytic system; the reusability and regeneration of the undissolved compound 1 are also investigated (shown in Scheme 2).^{71–75} Under the identical catalytic system with all the catalytic parameters fixed, we did the experiment three times with 10 mg of compound 1, which, at the end of each cycle, was filtered-off and collected and washed with CH_3CN

Scheme 2. Recycling Experiments of Compound 1



and then dried in air; the recovered catalyst was reused again directly. Each cycle experiment reveals that conversions are almost identical, but in the third cycle, the selectivity for styrene oxide decreased a little. After the last cycle experiment, we did the FT-IR and the PXRD analyses to compare whether the catalyst structure has changed or not. From Figure s6, we can see that due to the partial dissolution of compound 1, after three reaction cycles, the positions and intensities of both the FT-IR spectra and the PXRD patterns have somewhat changed but the main peak positions are just the same. Combined with the above views, it is indicated that compound 1 shows a good reusability for this catalytic system.

The energy problem has always been the hot spot of the scientific community, and the most important field is the renewable energy generation and storage.^{76–78} Electrochemical splitting of water can yield high-purity hydrogen, which is the cleanest fuel up to now. However, as for the process of electrolysis of water, the oxygen evolution reaction (OER) is a crucial and more difficult half-reaction. A lot of metallic oxides such as iridium oxide and ruthenium oxide have been studied as catalysts for a long time, and these studies have made great progress.^{79–81} While for these precious metal materials the higher cost is a serious problem, the cheaper materials for OER have become a key point and several different POMs^{82–85} and a Cu–en complex⁸⁶ as the electrochemical catalyst have also been tested. PONBs are a kind of excellent POM material, and there are also some reports about their electrochemical properties.^{29,87,88} However, the activity of the PONBs combined with Cu–en complexes for OER has not been studied yet. In this work, we take compounds 1–3 as the catalysts of OER, and all three catalysts exhibit good OER performances.⁸⁹

The OER performances of compounds 1–3 were evaluated in a traditional three-electrode system (modified carbon paste (CP) electrode, Pt wire, and Ag/AgCl (3 M KCl) electrode as the working, the counter and the reference electrodes, respectively) in 1 M KOH solution without *iR*-compensation. The result of linear sweep voltammetry (LSV) curves at the scan rate of 1 mV/s is depicted in Figure 6a. We take the two values (1 and 10 mA/cm²) of the current densities as the standards to evaluate the electrochemical water oxidation performances of the three compounds. From Scheme 3, we can see that at the 1 and 10 mA/cm² current densities the three compounds show different OER activities. And whether at 1 or 10 mA/cm², compound 3 exhibits the best water oxidation performances with the lowest overpotentials of 160 and 423 mV, respectively. As for the other two compounds, their required overpotentials are 187 and 516 mV for compound 1 and 173 and 436 mV for compound 2, respectively. The Tafel plots in Figure 6d were drawn using the LSV data; compared with compounds 1 and 3, compound 2 has a lower slope, which is 187 mV·dec⁻¹. So, despite compound 3 exhibiting the

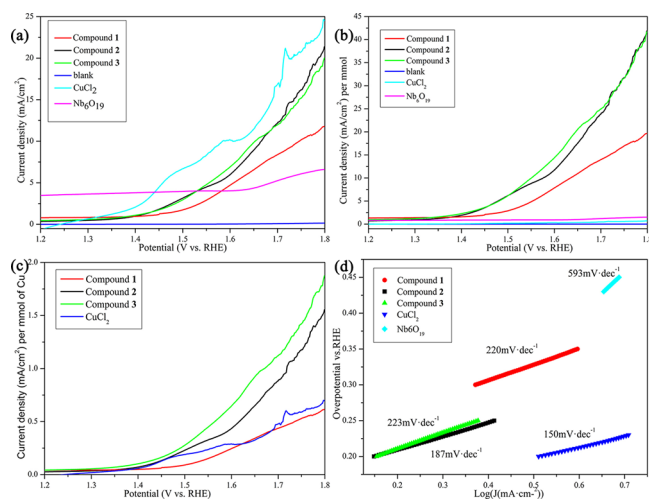
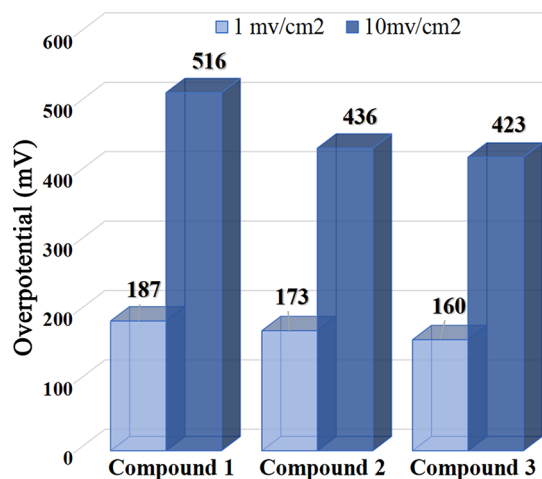


Figure 6. Electrochemical water oxidation performances of typical samples. (a) LSV curves of various catalysts in 1.0 M KOH without iR -compensation. (b) LSV curves for per formula μmol . (c) LSV curves for per Cu μmol . (d) Tafel plots derived from Figure 6a.

Scheme 3. Required Overpotentials for Current Densities of 1 and 10 mA/cm^2



lowest overpotential, compound 2 exceeded compound 3 in the current density at the end of the reaction due to the smaller Tafel slope. And the almost same slope may mean that compound 1 ($220 \text{ mV}\cdot\text{dec}^{-1}$) and compound 3 ($223 \text{ mV}\cdot\text{dec}^{-1}$) have a more similar catalytic mechanism. In addition, combined with the LSV and Tafel figures, CuCl_2 has an electrochemical performance more similar to those of the compounds 1–3 compared with $\{\text{Nb}_6\text{O}_{19}\}$. That implies perhaps the Cu is the catalytic active site for the three catalysts. And it is not surprising that CuCl_2 as the catalyst has a better result because it is unfair to compare CuCl_2 with our samples by weight (Figure 6a). The normalized current density data will show a fairer result, and the superiority of our catalysts is more obvious. As for the data we normalized by the compound formula weight, compounds 2 and 3 have similar best performances (Figure 6b), but if we take the Cu as the catalytic center and normalized by Cu, compound 3 will be the best one (Figure 6c). Besides, the electrochemical impedance spectroscopy (EIS) test is also strong evidence for the performances of the OERs. As we can see, compound 2 has a lower resistance, indicating a good conductivity that is

conducive to electron transfer (Figure s7). And the result is coincident with the Tafel slope. To evaluate the stability of the catalyst, we take the 10 h chronopotentiometric test of compound 1 at the overpotential of 270 mV (Figure s7). Unfortunately, the electrochemical stability of compound 1 is poor. At the end of the experiment when we treated the working electrode again in the 1 M KOH electrolyte, there is a phenomenon that the electrode can permeate into the solution. So, we speculate that the CP electrode, which is mechanically unstable and tends to expel some CPs from the electrode pocket into the solution (such a phenomenon was also observed by Galan-Mascaros et al.⁸²), cannot have a good stability under this condition in such a long-time test and cannot avoid its fragmentation, perhaps due to the relatively easy oxidation of the en ligand of the compounds. We hope we can improve the stability of the CP electrode by replacing the en ligand with the phenanthroline ligand (and its analogues) in the future.⁸⁵

However, the significant experimental difference between CuCl_2 and the Cu-PONb/CP electrodes was observed in the LSV data: the appearance of several additional precatalytic events in the CuCl_2 electrode (Figure 6a), which is absent for the Cu-PONb catalysts. Therefore, we speculate that the OER properties of the compounds originate from the synergistic interaction between the copper center of the coordinated copper complexes and the PONbs.⁸⁵

CONCLUSIONS

Three new compounds based on PONbs and copper coordination complexes have been synthesized and characterized. All three compounds not only can be used as catalysts for photocatalytic degradation of RhB under the simulated solar light irradiation but also can be used as oxidation catalysts in styrene oxidation and OER catalysts for water electrolysis. In following work, except the organic amine, we hope we can synthesize some new PONb compounds based on some more stable organic ligands like phenanthroline and so on and finally obtain some more stable catalysts of PONbs.

ASSOCIATED CONTENT

Supporting Information

The Supporting Information is available free of charge at <https://pubs.acs.org/doi/10.1021/acs.cgd.0c01193>.

Disordered copper complex of compound 1, polyhedron representation of $\{\text{Nb}_{24}\}$ clusters, details of bond valence sum calculations, FT-IR spectra, PXRD patterns, RhB photocatalytic performances, XRD patterns and IR spectra of compound 1 and the crystals of compound 1 after three consecutive epoxidation cycles, impedance plots, and chronoamperometry data of compound 1 (PDF)

Accession Codes

CCDC 2021807–2021809 contain the supplementary crystallographic data for this paper. These data can be obtained free of charge via www.ccdc.cam.ac.uk/data_request/cif, or by emailing data_request@ccdc.cam.ac.uk, or by contacting The Cambridge Crystallographic Data Centre, 12 Union Road, Cambridge CB2 1EZ, UK; fax: +44 1223 336033.

AUTHOR INFORMATION

Corresponding Author

Xiao-Bing Cui – College of Chemistry and State Key Laboratory of Inorganic Synthesis and Preparative Chemistry, Jilin University, Changchun, Jilin 130021, China; orcid.org/0000-0002-5254-7935; Email: cuixb@mail.jlu.edu.cn

Authors

Ting-Ting Zhang – College of Chemistry and State Key Laboratory of Inorganic Synthesis and Preparative Chemistry, Jilin University, Changchun, Jilin 130021, China

Guanghua Li – College of Chemistry and State Key Laboratory of Inorganic Synthesis and Preparative Chemistry, Jilin University, Changchun, Jilin 130021, China; orcid.org/0000-0003-3029-8920

Complete contact information is available at: <https://pubs.acs.org/10.1021/acs.cgd.0c01193>

Notes

The authors declare no competing financial interest.

ACKNOWLEDGMENTS

We are thankful for the grant from Jilin Provincial Department of science and technology (No. 20190802027ZG). We are thankful for helpful discussions from Dr. Xiao Zhang of Harbin Institute of Technology.

REFERENCES

- (1) Cronin, L.; Müller, A. From serendipity to design of polyoxometalates at the nanoscale, aesthetic beauty and applications. *Chem. Soc. Rev.* **2012**, *41*, 7333–7334.
- (2) Keggin, J. F. Structure of the molecule of 12-phosphotungstic acid. *Nature* **1933**, *131*, 908–909.
- (3) Müller, A.; Roy, S. En route from the mystery of molybdenum blue via related manipulatable building blocks to aspects of materials science. *Coord. Chem. Rev.* **2003**, *245*, 153–166.
- (4) Long, D. L.; Burkholder, E.; Cronin, L. Polyoxometalate clusters, nanostructures and materials: From self assembly to designer materials and devices. *Chem. Soc. Rev.* **2007**, *36* (36), 105–121.
- (5) Long, D. L.; Tsunashima, R.; Cronin, L. Polyoxometalates: Building Blocks for Functional Nanoscale Systems. *Angew. Chem., Int. Ed.* **2010**, *49*, 1736–1758.
- (6) Proust, A.; Matt, B.; Villanneau, R.; Guillemot, G.; Guozerh, G. L. P. Functionalization and post-functionalization: a step towards polyoxometalate-based materials. *Chem. Soc. Rev.* **2012**, *41*, 7605–7622.
- (7) Wang, S. S.; Yang, G. Y. Recent Advances in Polyoxometalate-Catalyzed Reactions. *Chem. Rev.* **2015**, *115*, 4893–4962.
- (8) Zhao, J. W.; Li, Y. Z.; Chen, L. J.; Yang, G. Y. Research progress on polyoxometalate-based transition-metal-rare-earth heterometallic derived materials: synthetic strategies, structural overview and functional applications. *Chem. Commun.* **2016**, *52*, 4418–4445.
- (9) Anyushin, A. V.; Kondinski, A.; Parac-Vogt, T. N. Hybrid polyoxometalates as post-functionalization platforms: from fundamentals to emerging applications. *Chem. Soc. Rev.* **2020**, *49*, 382–432.
- (10) Klemperer, W. G.; Marquart, T. A.; Yaghi, O. M. New directions in polyvanadate chemistry: from cages and clusters to baskets, belts, bowls, and barrels. *Angew. Chem., Int. Ed. Engl.* **1992**, *31*, 49–51.
- (11) Pope, M. T.; Müller, A. Polyoxometalate Chemistry: An Old Field with New Dimensions in Several Disciplines. *Angew. Chem., Int. Ed. Engl.* **1991**, *30*, 34–48.
- (12) Nyman, M.; Bonhomme, F.; Alam, T. M.; Bodriguez, M. A.; Cherry, B. R.; Krumhansl, J. L.; Nenoff, T. M.; Sattler, A. M. A general

synthetic procedure for heteropolyniobates. *Science* **2002**, *297*, 996–998.

(13) Dopta, J.; Mahnke, L. K.; Bensch, W. New pronounced progress in the synthesis of group 5 polyoxometalates. *CrystEngComm* **2020**, *22*, 3254–3268.

(14) Kinnan, M. K.; Creasy, W. R.; Fullmer, L. B.; Gibson, H. L. S.; Nyman, M. Nerve agent degradation with polyoxoniobates. *Eur. J. Inorg. Chem.* **2014**, *2014*, 2361–2367.

(15) Guo, W. W.; Lv, H. J.; Sullivan, K. P.; Gordon, W. O.; Balboa, A.; Wagner, G. W.; Musaev, D. G.; Bacsá, J.; Hill, C. L. Broad-Spectrum Liquid- and Gas-Phase Decontamination of Chemical Warfare Agents by One-Dimensional Heteropolyniobates. *Angew. Chem., Int. Ed.* **2016**, *55*, 7403–7407.

(16) Nyman, M.; Powers, C. R.; Bonhomme, F.; Alam, T. M.; Maginn, E. J.; Hobbs, D. H. Ion-Exchange behavior of one-dimensional linked dodecaniobate Keggin ion materials. *Chem. Mater.* **2008**, *20*, 2513–2521.

(17) Lin, Y. Y.; Zhang, J.; Zhu, Z. K.; Sun, Y. Q.; Li, X. X.; Zheng, S. T. An ultrastable {SiNb18O54}-based hybrid polyoxoniobate framework for selective removal of crystal violet from aqueous solution and proton-conduction. *Inorg. Chem. Commun.* **2020**, *113*, 107766.

(18) Zhang, Z. Y.; Lin, Q. P.; Kurunthu, D.; Wu, T.; Zuo, F.; Zheng, S. T.; Bardeen, C. J.; Bu, X. H.; Feng, P. Y. Synthesis and Photocatalytic Properties of a New Heteropolyoxyoniobate Compound: K10[Nb2O2(H2O)2][SiNb12O40] · 3 12H2O. *J. Am. Chem. Soc.* **2011**, *133*, 6934–6937.

(19) Hu, J. F.; Han, T.; Chi, Y. N.; Lin, Z. G.; Xu, Y. Q.; Yang, S.; Wei, D.; Zheng, Y. Z.; Hu, C. W. Sulfur-centred polyoxoniobate-based 3D organic-inorganic hybrid compound and its magnetic behavior. *Chem. Commun.* **2016**, *52*, 10846–10849.

(20) Shen, J. Q.; Wu, Q.; Zhang, Y.; Zhang, Z. M.; Li, Y. G.; Lu, Y.; Wang, E. B. Unprecedented High-Nuclear Transition-Metal-Cluster-Substituted Heteropolyoxyoniobates: Synthesis by {V8} Ring Insertion into the POM Matrix and Antitumor Activities. *Chem. - Eur. J.* **2014**, *20*, 2840–2848.

(21) Bonhomme, F.; Larentzos, J. P.; Alam, T. M.; Maqinn, E. J.; Nyman, M. Synthesis, structural characterization, and molecular modeling of dodecaniobate Keggin chain materials. *Inorg. Chem.* **2005**, *44*, 1774–1785.

(22) Li, C.; Zhao, D. Y.; Li, N.; Ma, Y. C.; Wei, G. L.; Wang, G.; Zhang, D. D. Dimeric dumbbell architecture based on PNb14 unit. *Inorg. Chem. Commun.* **2019**, *102*, 210–214.

(23) Huang, P.; Zhou, E. L.; Wang, X. L.; Sun, C. Y.; Wang, H. N.; Xing, Y.; Shao, K. Z.; Su, Z. M. New heteropolyniobates based on a bicapped Keggin-type {VNb14} cluster with selective adsorption and photocatalytic properties. *CrystEngComm* **2014**, *16*, 9582–9585.

(24) Zhang, T. T.; Lin, P. H.; Yu, G. Y.; Zhang, X.; Cui, X. B. Syntheses, characterization and properties of two new dodecaniobates presenting unprecedented features. *Dalton Trans.* **2020**, *49*, 6495–6503.

(25) Zhang, Z. Y.; Peng, J.; Shi, Z. Y.; Zhou, W. L.; Khan, S. U.; Liu, H. S. Antimony-dependent expansion for the Keggin heteropolyniobate family. *Chem. Commun.* **2015**, *51*, 3091–3093.

(26) Guo, G. L.; Xu, Y. Q.; Gao, J.; Hu, C. W. An unprecedented vanadoniobate cluster with 'trans-vanadium' bicapped Keggin-type {VNb12O40(VO)(2)}. *Chem. Commun.* **2011**, *47*, 9411–9413.

(27) Son, J. H.; Ohlin, C. A.; Johnson, R. L.; Yu, P.; Casey, W. H. A Soluble Phosphorus-Centered Keggin Polyoxoniobate with Bicapping Vanadyl Groups. *Chem. - Eur. J.* **2013**, *19*, 5191–5197.

(28) Zhang, T. T.; Zhang, X.; Lu, Y.; Li, G. D.; Xiao, L. N.; Cui, X. B.; Xu, J. Q. New organic-inorganic hybrid compounds based on [SiNb12V2O42](12-) with high catalytic activity for styrene epoxidation. *Inorg. Chem. Front.* **2017**, *4*, 1397–1404.

(29) Zhang, Y.; Shen, J. Q.; Zhang, L. H.; Zhang, Z. M.; Li, Y. X.; Wang, E. B. Four Polyoxoniobate-Based Inorganic-Organic Hybrids Assembly from Bicapped Heteropolyoxyoniobate with Effective Antitumor Activity. *Cryst. Growth Des.* **2014**, *14*, 110–116.

(30) Li, N.; Liu, Y. W.; Lu, Y.; He, D. F.; Liu, S. M.; Wang, X. Q.; Li, Y. G.; Liu, S. X. An arsenicniobate-based 3D framework with selective

adsorption and anion-exchange properties. *New J. Chem.* **2016**, *40*, 2220–2224.

(31) Shen, J. Q.; Zhang, Y.; Zhang, Z. M.; Li, Y. G.; Gao, Y. Q.; Wang, E. B. Polyoxoniobate-based 3D framework materials with photocatalytic hydrogen evolution activity. *Chem. Commun.* **2014**, *50*, 6017–6019.

(32) Liang, Z. J.; Li, T. T.; Zhang, L.; Zheng, L. J.; Jia, W. N.; Mao, Q. H. Synthesis and characterization of two hexacopper-capped Keggin-type polyoxoniobates. *Inorg. Chem. Commun.* **2020**, *116*, 107895.

(33) Müsscher-Polzin, P.; Näther, C.; Bensch, W. A hexaniobate expanded by six [Hg(cyclam)]²⁺ complexes via Hg–O bonds yields a positively charged polyoxoniobate cluster. *Z. Naturforsch., B: J. Chem. Sci.* **2020**, *75*, 233–237.

(34) Müsscher-Polzin, P.; Näther, C.; Bensch, W. Room Temperature Synthesis, Crystal Structure, Water Sorption, and Thermal and Electronic Properties of {[Cu(phen)]₂[Cu(phen)₂]₂Nb₆O₁₉·24H₂O}. *Cryst. Growth Des.* **2021**, *21*, 156–165.

(35) Wang, J. P.; Niu, H. Y.; Niu, J. Y. A novel Lindqvist type polyoxoniobate coordinated to four copper complex moieties: {Nb₆O₁₉[Cu(2,2'-bipy)]₂[Cu(2,2'-bipy)₂]₂·19H₂O}. *Inorg. Chem. Commun.* **2008**, *11*, 63–65.

(36) Niu, J. Y.; Fu, X.; Zhao, J. W.; Li, S. Z.; Ma, P. T.; Wang, J. P. Two-Dimensional Polyoxoniobates Constructed from Lindqvist-Type Hexaniobates Functionalized by Mixed Ligands. *Cryst. Growth Des.* **2010**, *10*, 3110–3119.

(37) Dopta, J.; Hansen, A.; Pienack, N.; Mahnke, L. K.; Reinsch, H.; Etter, M.; Näther, C.; Bensch, W. Bond Formation upon Water Removal in an Unusual “Pseudo”-Topotactic Reaction Investigated by Single-Crystal Structure and in Situ Synchrotron X-ray Powder Diffraction Analysis. *Cryst. Growth Des.* **2019**, *19*, 5743–5750.

(38) Dopta, J.; Krause, D.; Näther, C.; Bensch, W. Controlling Fast Nucleation and Crystallization of Two New Polyoxoniobates. *Cryst. Growth Des.* **2018**, *18*, 4130–4139.

(39) Dopta, J.; Grzanna, S.; Näther, C.; Bensch, W. On the influence of the titanium source on the composition and structure of novel titanoniobates. *Dalton Trans.* **2018**, *47*, 15103–15113.

(40) Maekawa, M.; Ozawa, Y.; Yagasaki, A. Icosaniobate: A new member of the isoniobate family. *Inorg. Chem.* **2006**, *45*, 9608–9609.

(41) Huang, P.; Qin, C.; Wang, X. L.; Sun, C. Y.; Yang, G. S.; Shao, K. Z.; Jiao, Y. Q.; Zhou, K.; Su, Z. M. An unprecedented organic-inorganic hybrid based on the first {Nb₁₀V₄O₄₀(OH)₂}₁₂- clusters and copper cations. *Chem. Commun.* **2012**, *48*, 103–105.

(42) Huang, P.; Qin, C.; Su, Z. M.; Xing, Y.; Wang, X. L.; Shao, K. Z.; Lan, Y. Q.; Wang, E. B. Self-Assembly and Photocatalytic Properties of Polyoxoniobates: {Nb₂₄O₇₂}, {Nb₃₂O₉₆}, and {K₁₂Nb₉₆O₂₈₈} Clusters. *J. Am. Chem. Soc.* **2012**, *134*, 14004–14010.

(43) Zhu, Z. K.; Lin, Y. Y.; Yu, H.; Li, X. X.; Zheng, S. T. Inorganic-organic hybrid polyoxoniobates: polyoxoniobate metal complex cage and cage framework. *Angew. Chem., Int. Ed.* **2019**, *58*, 16864–16868.

(44) Bontchev, R. P.; Nyman, M. Evolution of polyoxoniobate cluster anions. *Angew. Chem., Int. Ed.* **2006**, *45*, 6670–6672.

(45) Wang, J. P.; Niu, H. Y.; Niu, J. Y. Preparation, crystal structure, and characterization of an inorganic-organic hybrid polyoxoniobate [Cu(en)₂]₃[Cu(en)₂(H₂O)]₁·5[KO·5Nb₂₄O₇₂H₁₄·5]₂·25H₂O. *Proc. - Indian Acad. Sci., Chem. Sci.* **2008**, *120*, 309–313.

(46) Niu, J. Y.; Ma, P. T.; Niu, H. Y.; Li, J.; Zhao, J. W.; Song, Y.; Wang, J. P. Giant Polyniobate Clusters Based on [Nb₇O₂₂]₉- Units Derived from a Nb₆O₁₉ Precursor. *Chem. - Eur. J.* **2007**, *13*, 8739–8748.

(47) Wang, Z. L.; Tan, H. Q.; Chen, W. L.; Li, Y. G.; Wang, E. B. A copper(ii)-ethylenediamine modified polyoxoniobate with photocatalytic H₂ evolution activity under visible light irradiation. *Dalton Trans.* **2012**, *41*, 9882–9884.

(48) Liang, Z. J.; Sun, J. J.; Zhang, D. D.; Ma, P. T.; Zhang, C.; Niu, J. Y.; Wang, J. P. Assembly of TeO₃²⁻ Ions Embedded in an Nb/O Cage with Selective Decolorization of Organic Dye. *Inorg. Chem.* **2017**, *56*, 10119–10122.

(49) Filowitz, M.; Ho, R. K. C.; Klemperer, W. G.; Shum, W. Oxygen-17 nuclear magnetic resonance spectroscopy of polyoxometalates. I. Sensitivity and resolution. *Inorg. Chem.* **1979**, *18*, 93–103.

(50) Sheldrick, G. M. A short history of SHELX. *Acta Crystallogr., Sect. A: Found. Crystallogr.* **2008**, *64*, 112–122.

(51) Sheldrick, G. M. Crystal structure refinement with SHELXL. *Acta Crystallogr., Sect. C: Struct. Chem.* **2015**, *71*, 3–8.

(52) Dolomanov, O. V.; Bourhis, L. J.; Gildea, R. J.; Howard, J. A. K.; Puschmann, H. OLEX2: A complete structure solution, refinement and analysis program. *J. Appl. Crystallogr.* **2009**, *42*, 339–341.

(53) Müller, A.; Beckmann, E.; Bögge, H.; Schmidtman, M.; Dress, A. Inorganic Chemistry Goes Protein Size: A Mo₃₆₈ Nano-Hedgehog Initiating Nanochemistry by Symmetry Breaking. *Angew. Chem., Int. Ed.* **2002**, *41*, 1162–1167.

(54) Hagrman, P. J.; Zubieta, J. Solid-state coordination chemistry: Influences of {M(terpyridyl)} (M = Ni(III), Cu(II), Ni(II)) subunits on molybdenum oxide structures. *Inorg. Chem.* **2000**, *39*, 5218–5224.

(55) Lü, J.; Lin, J. X.; Zhao, X. L.; Cao, R. Photochromic hybrid materials of cucurbituril and polyoxometalates as photocatalysts under visible light. *Chem. Commun.* **2012**, *48*, 669–671.

(56) Sha, J. Q.; Sun, J. W.; Li, M. T.; Wang, C.; Li, G. M.; Yan, P. F.; Sun, L. J. Secondary spacer modulated assembly of polyoxometalate based metal-organic frameworks. *Dalton Trans.* **2013**, *42*, 1667–1677.

(57) Pang, H. J.; Ma, H. Y.; Peng, J.; Zhang, C. J.; Zhang, P. P.; Su, Z. M. Study of a hydrothermal reaction system of copper, imidazole and polyoxometalates: selective assembly of a 3D porous metal-organic pseudo-rotaxane framework and encapsulation of polyoxometalate clusters. *CrystEngComm* **2011**, *13*, 7079–7085.

(58) Hu, Y.; Luo, F.; Dong, F. F. Design synthesis and photocatalytic activity of a novel lilac-like silver-vanadate hybrid solid based on dicyclic rings of [V₄O₁₂]₄- with [Ag₇]₇₊ cluster. *Chem. Commun.* **2011**, *47*, 761–763.

(59) Wang, X. L.; Zhao, D.; Tian, A. X.; Ying, J. Three 3D silver-bis(triazole) metal-organic frameworks stabilized by high-connected Wells-Dawson polyoxometalates. *Dalton Trans.* **2014**, *43*, 5211–5220.

(60) Johnson, B. J. S.; Stein, A. Surface modification of mesoporous, macroporous, and amorphous silica with catalytically active polyoxometalate clusters. *Inorg. Chem.* **2001**, *40*, 801–808.

(61) Neumann, R.; Miller, H. Alkene oxidation in water using hydrophobic silica particles derivatized with polyoxometalates as catalysts. *J. Chem. Soc., Chem. Commun.* **1995**, 2277–2278.

(62) Wang, J.; Zou, Y. C.; Sun, Y.; Hemgesberg, M.; Schaffner, D.; Gao, H. C.; Song, X. J.; Zhang, W. X.; Jia, M. J.; Thiel, W. R. Electrostatic immobilization of phosphomolybdic acid on imidazolium-based mesoporous organosilicas for catalytic olefin epoxidation. *Chin. J. Catal.* **2014**, *35*, 532–539.

(63) Song, X. J.; Zhu, W. C.; Li, K. G.; Wang, J.; Niu, H. L.; Gao, H. C.; Gao, W. X.; Zhang, W. X.; Yu, J. H.; Jia, M. J. Epoxidation of olefins with oxygen/isobutyraldehyde over transition-metal-substituted phosphomolybdic acid on SBA-15. *Catal. Today* **2016**, *259*, 59–65.

(64) Li, S. J.; Ji, P. P.; Han, S. N.; Hao, Z. M.; Chen, X. N. Two polyoxoniobates-based ionic crystals as Lewis base catalysts for cyanosilylation. *Inorg. Chem. Commun.* **2020**, *111*, 107666.

(65) Hu, J. F.; Dong, J.; Huang, X. Q.; Chi, Y. N.; Lin, Z. G.; Li, J. K.; Yang, S.; Ma, H. W.; Hu, C. W. Immobilization of Keggin polyoxovanadoniobate in crystalline solids to produce effective heterogeneous catalysts towards selective oxidation of benzyl-alkanes. *Dalton Trans.* **2017**, *46*, 8245–8251.

(66) Monnier, J. R. The direct epoxidation of higher olefins using molecular oxygen. *Appl. Catal., A* **2001**, *221*, 73–91.

(67) Cancino, P.; Paredes-García, V.; Aguirre, P.; Spodine, E. A reusable CuII based metal-organic framework as a catalyst for the oxidation of olefins. *Catal. Sci. Technol.* **2014**, *4*, 2599–2607.

(68) De, S. R.; Kumar, G.; Jat, J. L.; Birudaraju, S.; Lu, B.; Manne, R.; Puli, N.; Adebisin, A. M.; Falck, J. R. Regio- and Stereoselective Monoepoxidation of Dienes using Methyltrioxorhenium: Synthesis of Allylic Epoxides. *J. Org. Chem.* **2014**, *79*, 10323–10333.

- (69) Neumann, R.; Gara, M. The Manganese-Containing Polyoxometalate, $[WZnMnn_2(ZnW9O34)_2]^{12-}$, as a Remarkably Effective Catalyst for Hydrogen Peroxide Mediated Oxidations. *J. Am. Chem. Soc.* **1995**, *117*, 5066–5074.
- (70) Choudhary, V. R.; Jha, R.; Jana, P. Selective epoxidation of styrene to styrene oxide by TBHP using simple transition metal oxides (NiO, CoO or MoO₃) as highly active environmentally-friendly catalyst. *Catal. Commun.* **2008**, *10*, 205–207.
- (71) Amarante, T. R.; Neves, P.; Valente, A. A.; Paz, F. A. A.; Fitch, A. N.; Pillinger, M.; Gonçalves, I. S. Hydrothermal Synthesis, Crystal Structure, and Catalytic Potential of a One-Dimensional Molybdenum Oxide/Bipyridinedicarboxylate Hybrid. *Inorg. Chem.* **2013**, *52*, 4618–4628.
- (72) Abrantes, M.; Amarante, T. R.; Antunes, M. M.; Gago, S.; Paz, F. A. A.; Margiolaki, I.; Rodrigues, A. E.; Pillinger, M.; Valente, A. A.; Gonçalves, I. S. Synthesis, Structure, and Catalytic Performance in Cyclooctene Epoxidation of a Molybdenum Oxide/Bipyridine Hybrid Material: $\{[MoO_3(bipy)][MoO_3(H_2O)]\}_n$. *Inorg. Chem.* **2010**, *49*, 6865–6873.
- (73) Amarante, T. R.; Neves, P.; Gomes, A. C.; Nolasco, M. M.; Ribeiro-Claro, P.; Coelho, A. C.; Valente, A. A.; Paz, F. A. A.; Smeets, S.; McCusker, L. B.; Pillinger, M.; Gonçalves, I. S. Synthesis, Structural Elucidation, and Catalytic Properties in Olefin Epoxidation of the Polymeric Hybrid Material $[Mo_3O_9(2-[3(5)\text{-Pyrazolyl}]\text{pyridine})]_n$. *Inorg. Chem.* **2014**, *53*, 2652–2665.
- (74) Neves, P.; Amarante, T. R.; Gomes, A. C.; Coelho, A. C.; Gago, S.; Pillinger, M.; Gonçalves, I. S.; Silva, C. M.; Valente, A. A. Heterogeneous oxidation catalysts formed in situ from molybdenum tetracarbonyl complexes and tert-butyl hydroperoxide. *Appl. Catal., A* **2011**, *395*, 71–77.
- (75) Abrantes, M.; Gonçalves, I. S.; Pillinger, M.; Vurchio, C.; Cordero, F. M.; Brandi, A. Molybdenum oxide/bipyridine hybrid material $\{[MoO_3(bipy)][MoO_3(H_2O)]\}_n$ as catalyst for the oxidation of secondary amines to nitrones. *Tetrahedron Lett.* **2011**, *52*, 7079–7082.
- (76) Liu, L. Z.; Ci, S. Q.; Bi, L. L.; Jia, J. C.; Wen, Z. H. Three-dimensional nanoarchitectures of Co nanoparticles inlaid on N-doped macroporous carbon as bifunctional electrocatalysts for glucose fuel cells. *J. Mater. Chem. A* **2017**, *5*, 14763–14774.
- (77) Wu, H. B.; Lou, X. W. Metal-organic frameworks and their derived materials for electrochemical energy storage and conversion: Promises and challenges. *Sci. Adv.* **2017**, *3*, No. eaap9252.
- (78) Suntivich, J.; Gasteiger, H. A.; Yabuuchi, N.; Nakanishi, H.; Goodenough, J. B.; Shao-Horn, Y. Design principles for oxygen-reduction activity on perovskite oxide catalysts for fuel cells and metal-air batteries. *Nat. Chem.* **2011**, *3*, 546–550.
- (79) Yagi, M.; Tomita, E.; Kuwabara, T. Remarkably high activity of electrodeposited IrO₂ film for electrocatalytic water oxidation. *J. Electroanal. Chem.* **2005**, *579*, 83–88.
- (80) Blakemore, J. D.; Schley, N. D.; Olack, G. W.; Incarvito, C. D.; Brudvig, G. W.; Crabtree, R. H. Anodic deposition of a robust iridium-based water-oxidation catalyst from organometallic precursors. *Chem. Sci.* **2011**, *2*, 94–98.
- (81) Lee, Y. M.; Suntivich, J.; May, K. J.; Perry, E. E.; Shao-Horn, Y. Synthesis and Activities of Rutile IrO₂ and RuO₂ Nanoparticles for Oxygen Evolution in Acid and Alkaline Solutions. *J. Phys. Chem. Lett.* **2012**, *3*, 399–404.
- (82) Blasco-Ahicart, M.; Soriano-López, J.; Carbó, J. J.; Poblet, J. M.; Galan-Mascaros, J. R. Polyoxometalate electrocatalysts based on earth-abundant metals for efficient water oxidation in acidic media. *Nat. Chem.* **2018**, *10* (1), 24–30.
- (83) Yin, Q. S.; Tan, J. M.; Besson, C.; Geletii, Y. V.; Musaev, D. G.; Kuznetsov, A. E.; Luo, Z.; Hardcastle, K. I.; Hill, C. L. A Fast Soluble Carbon-Free Molecular Water Oxidation Catalyst Based on Abundant Metals. *Science* **2010**, *328*, 342–345.
- (84) Du, Y.; Yu, T.; Fu, Z.; Bi, L. H. A multilayer assembly of two mixed-valence Mn¹⁶-containing polyanions and study of their electrocatalytic activities towards water oxidation. *Dalton Trans.* **2018**, *47*, 7282–7289.
- (85) Singh, C.; Mukhopadhyay, S.; Das, S. K. Polyoxometalate-Supported Bis(2,2'-bipyridine)mono(aqua)nickel(II) Coordination Complex: an Efficient Electrocatalyst for Water Oxidation. *Inorg. Chem.* **2018**, *57*, 6479.
- (86) Liu, X.; Cui, S. S.; Qian, M. M.; Sun, Z. J.; Du, P. W. In situ generated highly active copper oxide catalysts for the oxygen evolution reaction at low overpotential in alkaline solutions. *Chem. Commun.* **2016**, *52*, 5546–5549.
- (87) Ong, G. K.; Cabezas, C. A. S.; Dominguez, M. N.; Skjærvø, S. L.; Heo, S.; Milliron, D. J. Electrochromic Niobium Oxide Nanorods. *Chem. Mater.* **2020**, *32*, 468–475.
- (88) Guo, G. L.; Xu, Y. Q.; Gao, J.; Hu, C. W. The $\{V_4Nb_6O_{30}\}$ Cluster: A New Type of Vanadoniobate Anion Structure. *Chem. - Eur. J.* **2012**, *18*, 3493–3497.
- (89) Tahir, M.; Pan, L.; Idrees, F.; Zhang, X. W.; Wang, L.; Zou, J. J.; Wang, Z. L. Electrocatalytic oxygen evolution reaction for energy conversion and storage: A comprehensive review. *Nano Energy* **2017**, *37*, 136–157.